International Journal of Advanced Research in Physical Science (IJARPS)
Volume 2, Issue 3, March 2015, PP 7-21
ISSN 2349-7874 (Print) & ISSN 2349-7882 (Online)
www.arcjournals.org

Dielectric Spectroscopy Studies on Lead Sodium Bismuth Potasium Neobate (PNBKN) Ceramic

D.Gangadharudu
S.R.V.B.S.J.B.M.R.College, Peddapuram
dhard98@gmail.com

Y.N.Ch.Ravi Babu
The Hindu College
Machilipatnam

B.Venkateswara Rao
S S & N College, Narasaraopeta

K.Srinivasa Rao
V.S.M. College, Ramachandrapuram

Abstract: *Dielectric response, impedance, modulus, dc and ac conductivity of polycrystalline ceramic, $Pb_{0.65}Na_{0.075}Bi_{0.075}K_{0.4}Nb_2O_6$ (PNBKN) at different temperatures (35^0C-600^0C) and frequencies (45Hz -5MHz) has been carried out. PNBKN prepared by solid state reaction technique, the results of X-ray diffraction confirmed the partial substitution of Sodium and Bismuth at A-site, in TB type structure lead potassium niobate ($Pb_{(1-X)}$ $K_{2X}Nb_2O_6$, PKN, X=0.2) doesn't distort its structure, but phase transition temperature found to be decreased to 325^0C compared to PKN. The dielectric analysis reveals the presence of electrode polarization, free charge motion at low frequencies which are related to space charge polarization and conductivity relaxation respectively. Complex impedance plots (Cole –Cole plots) showed a non –Debye type relaxation. These are resolved into three semicircles, indicating the bulk, grain boundary and interfacial polarization effects. Modulus studies confirm the electrode and/or ionic polarization effect by hopping and localized motion of ions. Ac conductivity has been found to be frequency dependent at high frequency and low temperatures such as $\sigma = \sigma_{dc} + A\omega^S$, and shows frequency independent at low frequencies and high temperatures. DC and AC conductivity activation energies were estimated on the material and the results are discussed.*

Keywords: *Ceramic, Dielectric, Impedance, Electric Modulus, Conductivity.*

1. INTRODUCTION

Ferroelectric compounds related to the tetragonal tungsten bronze (TTB) have received a great deal of attention, mainly due to their potential electro-optical and photo-refractive applications. One of the most promising compounds in this large family is lead potassium niobate ($Pb_2KNb_5O_{15}$, PKN), which shows high piezoelectric and electromechanical coupling constants and could be a desirable material for surface acoustic wave applications [1-2]. However, the utilization of PKN single crystals is largely limited due to PbO loss resulting from the high-temperature growth and to formation of cracks when cooling through the Curie temperature [3]. Several attempts have been made to elaborate PKN ceramics, but microstructure and stoichiomerty have always remained difficult to control [4-7]. Pb-K- niobate ($Pb_{1-x}K_{2x}Nb_2O_6$) series is a limited solid solution between Pb-niobate ($PbNb_2O_6$) and K- niobate ($KNbO_3$) for x varying from 0 to 0.34[8]. Two members of the PKN series with x=0.23 and x=0.34 were processed and reported their structure and dielectric properties [9]. Ac impedance spectroscopy (IS) is a well-known technique for investigating the electrical behavior of electrochemical cells and ionically conducting materials such as polymers, ceramics and glasses. Impedance spectroscopy analysis of ceramic materials enables separation of bulk and boundary components of the conductivity [10, 11].

Rao et al., reported [12] the dielectric, impedance, electric modulus and conductivity studies on PKN for x=0.20. However, dielectric and impedance spectroscopy studies have not been found in literature on the substitution of Sodium and Bismuth in PKN to understand the electrical relaxation.

The subject of the present paper is to study the electrical properties of$Pb_{0.65}Na_{0.075}Bi_{0.075}K_{0.4}Nb_2O_6$ (PNBKN) niobate ceramics. The impedance and dielectric data are analyzed to understand the electrical relaxation of these ceramics. Also, we present the results on ac and dc conductivity measurements on this material.

2. EXPERIMENTAL

The ceramic material of Lead sodium bismuth potassium niobate, with general formula $Pb_{1-x-y}(Na_{0.5}Bi_{0.5})_yK_{2x}Nb_2O_6$ (PNBKN), where x=0.20 and y=0.15 has been prepared by double sintering technique. The raw materials, PbO, Na_2CO_3, Bi_2O_3, K_2CO_3 and Nb_2O_5 are of analar grade have been taken for the preparation of the ceramic compositions.

An excess of 6 wt% of PbO and 4.5wt% of Bi_2O_3 have been added to the composition to compensate the loss of lead and bismuth due to evaporation on heating. The vapor pressure of Bismuth oxide, Bi_2O_3 (750mm Hg at 570^0C) is on the order to that of lead oxide (750mm Hg at 760^0C) [13].

The weighed powders were grounded in an agate mortar and pestle for more than 8 Hrs. A small quantity of methanol is added to achieve thorough homogeneity of the mixture and the resultant slurry was well grounded until all methanol evaporated. The physical mixture was calcined at 900^0C for 4 Hrs. The procedure has been repeated three times with an intermediate hand grinding to ensure the completion of the reaction [14]. Binder (Polyvinyl alcohol 5 wt %) mixed with calcined powder and shaped to a disk form at a pressure of 500 MPa. Sintered the disk material at 1200^0C/60 min in air. Silver electrodes were coated on the both sides of the pellete, which are 10 mm in diameter and 2 mm in thickness and heated on hotplate for 30 min. The electrical and dielectric properties of the sample was carried out by a computer controlled HIOKI LCR Hitester model 3532 over a wide frequency range (45Hz – 5MHz) and in the temperature range ($35 – 590^0$C).

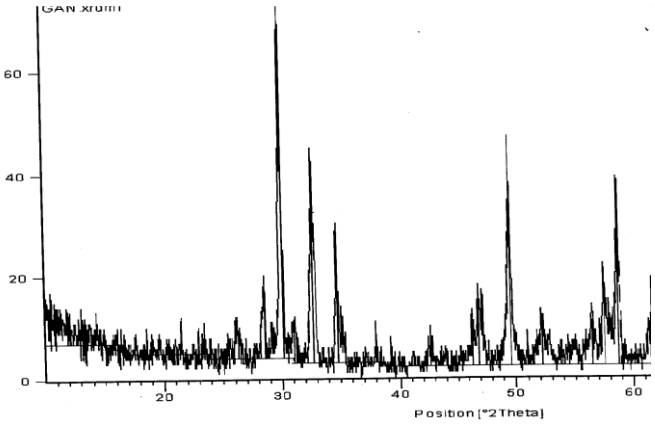

Fig1. *XRD patterns of PNBKN*

The X – ray diffraction patterns obtained on PNBKN compositions have been shown in the Figure 1. XRD has been studied for $2\theta = 10$ to 60^0. The XRD patterns have been indexed by POWD – an interactive powder diffraction data interpretation and indexing program version 2.2–by E.W.Yu, School of Physical Sciences, Flinders University of South Australia, Bedford, SA 5042, Australia. Powder XRD analysis showed the composition under investigation is homogeneous and single phase with orthorhombic structure. The X-ray diffractogram on PNBKN is shown in Fig.1.

The values of lattice parameters obtained are given in table 1. From the table1, the lattice parameters, are a=17.760Å, b =18.231Å and c = 3.925 Å on PNBKN. Jana et. al., [15] reported, the lattice parameters, a = 17.723 Å, b = 17.987 Å and c=3.895

Table1. *Lattice parameters of PNBKN*

composition	Lattice Parameters (Å)	Cell Volume $(Å)^3$	Orthorhombic distortion (b/a)	Density (g/cm^3)		Porosity	% density
				X-Ray	Exptl		
PNBKN	a = 17.760 b = 18.231 c = 3.925	1270.8	1.026	5.83	5.64	0.034	96.6

Å in single crystal, $Pb_{0.8}K_{0.4}Nb_2O_6$. Rao et. al [12] reported, PKN has orthorhombic structure with lattice parameters, a=17.721Å, b=17.983Å and c=3.892Å in ceramic, $Pb_{0.8}K_{0.4}Nb_2O_6$. The values of lattice parameters obtained in the present investigation are very much closer to the reported which is almost coincides with the T_C of the material. Curie-Weiss law has been verified in the para region and the Curie constant (K) is obtained to be the order of 10^5, revealing the materials belongs to oxygen octahedra for example: Barium strontium sodium Niobate (BSSN) and Lead Barium Niobate (PBN) [16, 17]. The values of room temperature dielectric constant ε^1RT, T^0C, dielectric constant at T_c ε^1T_c, Curie constant (K) and dielectric loss at room temperature (tanδ) are given in table. 2.

Table2. *Dielectric Data at 1 KHz*

Composition	ϵ^1_{RT}	ϵ^1_{TC}	T_C ^oC	K ^oC	Tanδ
PNBKN	787	1598	340	$0.8x10^5$	0.03

However, there is a increase in the value of lattice parameters in PNBKN because of the substitution od Sodium and Bismuth ions in PKN. The density about 96.6% to that of theoretical value obtained indicating the material has been sintered well.

3. DIELECTRICS

Real part of dielectric constant (εl) versus temperature at 500 Hz, 1KHz, 10KHz and 20KHz on the composition is shown in figures 2 (a). A phase transition from ferroelectric to paraelectric is observed in the composition at 340^0C (figures 2(a)). Further, no shift in T_C has been observed at different frequencies, revealing the material belongs to traditional ferroelectric but not relaxor. Dependence of imaginary part of dielectric constant (ε^{ll}) with temperature at 500 Hz, 1 KHz, 10 KHz and 20 KHz on PNBKN is shown in figures 2(b). A certain anomaly in ε^{ll} versus temperature has been observed

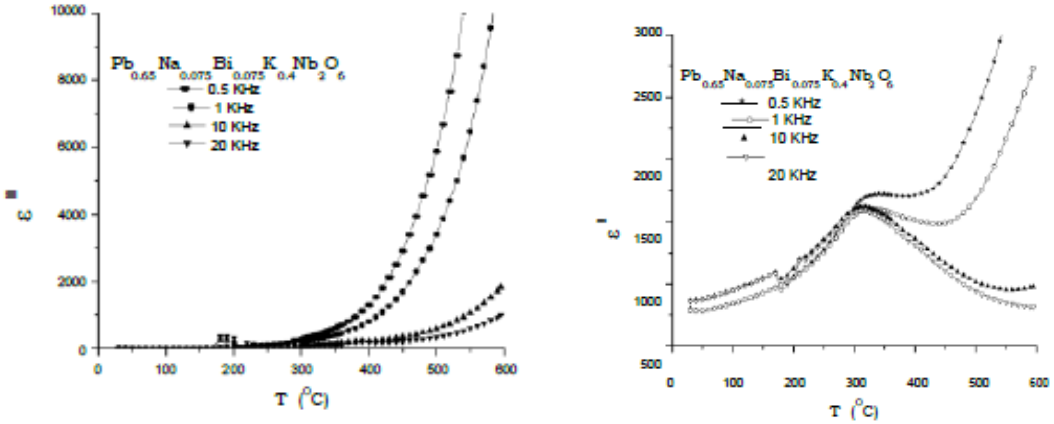

(a) (b)

Fig2 (a, b). *Variation of real part of dielectric constant (ε^l) and imaginary part of dielectric constant (ε^{ll}) as function of temperature.*

Figure3 shows the variation of ε^l and ε^{ll} with log f at different temperatures on material. As temperature increases a sudden raise in the values of ε^{ll} and ε^l is observed and both curves intersect, and their intersecting frequency shifts to higher frequency side. At 300^0C the values of ε^l and ε^{ll} differ. The value of ε^l and ε^{ll} at 45 Hz is nearly same and they started at 300 at measured temperature of 340^0C. As the temperature increases the values of ε^l and ε^{ll} increases and intersects. Further, increase in temperature the intersection of ε^l and ε^{ll} moves towards higher frequency side. Both ε^l and ε^{ll} exhibits high values, which reveals the effect of space charge polarization, and/or conducting ion motion. It is well known that in the conducting dielectric materials, high ε^l values may be interpreted as the accumulation of charges at the interface between the sample and electrode, i.e. space charge polarization. The high values of ε^{ll} at low frequencies in the present materials may be due to free charge motion and thus may be related to Ac conductivity relaxation.

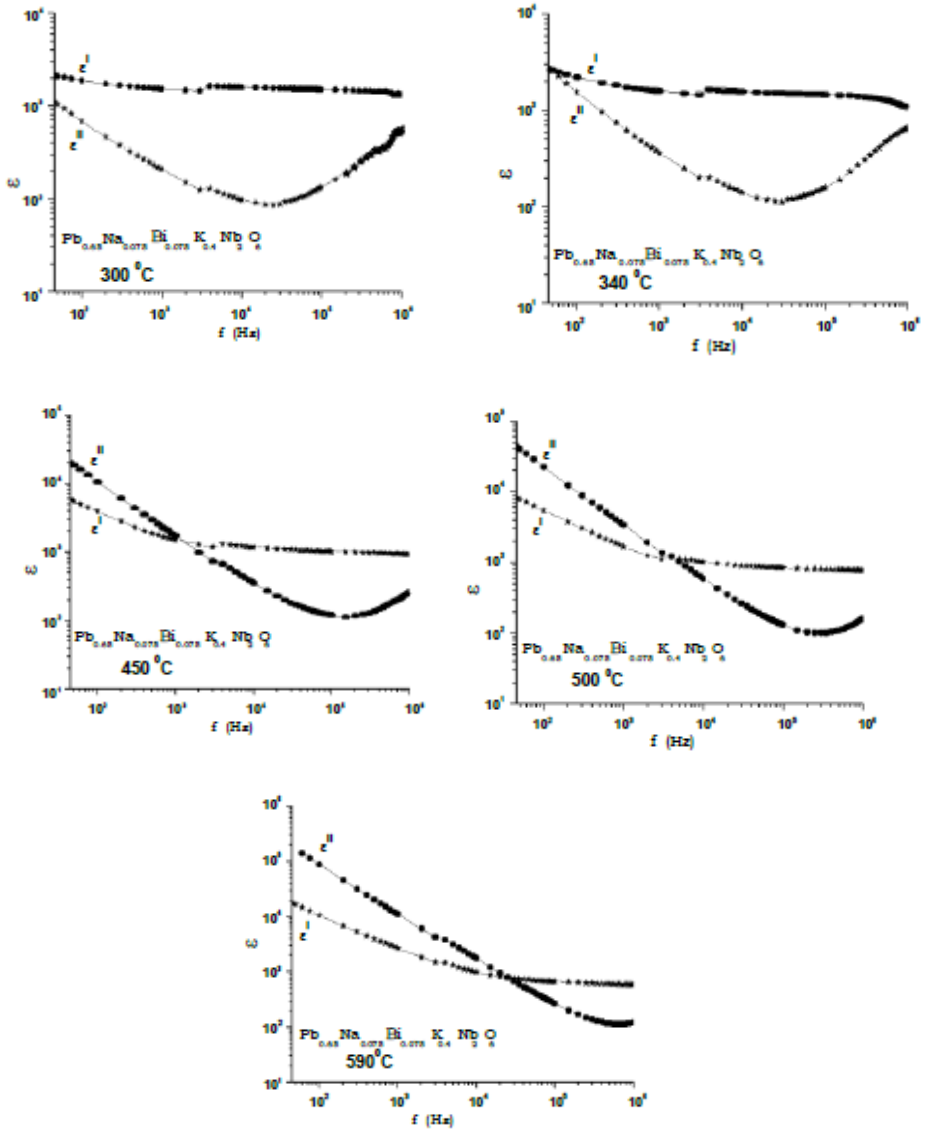

Fig3. *Variation of real and imaginary part of dielectric constant (ε^{I} and ε^{II}) with log f at different temperatures on PNBKN.*

The complex dielectric constant as a function of the frequency ω in accordance with the Jonscher's powerlaw is given by the following expression.

$$\varepsilon^* = \varepsilon_r^{1} - i\,\varepsilon_r^{11} = \varepsilon_\infty + \sigma / i\varepsilon_0\,\omega + (a(T) / \varepsilon_0)\,(i\,\omega^{n(T)-1})$$

Where ε_∞ is the high frequency value of the dielectric constant, n(T) is the temperature dependent exponent and a(T) determines the strength of the polarizability arising from the universal mechanism. The temperature and frequency dependencies of ε^{1} yield a straight line for a constant n with a slope equal to n-1 in double logarithmic plot.

A unit value of n implies a Debye case, and it is attainable [18] at very low temperatures. However, as the temperature increases, the interaction between the charge carriers participating in the polarization process increases, leading to a decrease in n. The value of n calculated from the high frequency region decreases as the temperature increases and attains a minimum near T_C and subsequently it increases with further increase in temperature. The observed minimum at Tc implies the strong interaction between the charge carriers and the lattice. At high frequencies the charge carriers fail to respond to the external field, therefore the measured dielectric constant is due to the contribution from the lattice polarization. This accounts for a linear decrease in the low frequency region and a frequency- independent plateau region at high frequencies. The temperature dependence of n(T) is shown in Fig. 4.

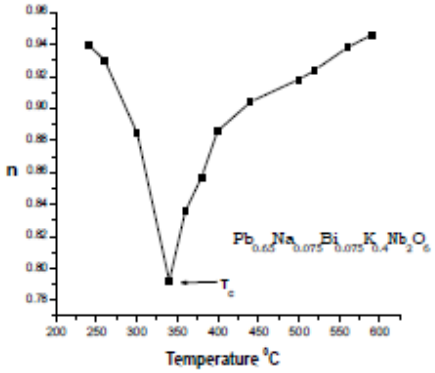

Fig4. *Variation of the critical exponent n(T) with temperature showing a minimum at T_C on PNBKN.*

The exponent n(T) decreases with increase in temperature and rapidly falls to a minimum at T_C and subsequently increases with further increase in temperature. The possible way of explaining the observed minimum at T_C is to consider the interaction of the charge carriers with the lattice. These results are in line with those reported for ferroelectric $Pb_2KNb_4TaO_{15}$ by Lu et al. [19].

4. IMPEDANCE SPECTROSCOPY

The application of the A.C technique of the complex impedance analysis [20, 21] eliminates the pseudo effects, if any, in the material electrical properties by separating out the real and imaginary parts of the material electrical properties. It has unique feature to investigate the electrical properties of a material, which are independent of the sample geometrical factors and thereby enables a better correlation of electrical properties with sample microstructure [22].

Complex impedance diagrams have been found to be very useful to distinguish the contribution of resistivity from grain and grain boundaries of polycrystalline sample having different time constants in frequency domain [22]. Impedance and modulus spectroscopy is promising non destructive testing method for analyzing ferroelectrics and piezo- electrics. The literature survey indicates lot of work in variety of materials has been characterized for electrical properties using this complex impedance and modulus formalism [23].

Figure 5 shows the variation of real part of the impedance (Z') as a function of frequency at different temperatures (400 -590^{0}C). From the figure 5 there is a monotonous decrease in the Z^1 with rise in frequency and attains a constant value above a certain frequency. It has been noticed Z^1 values decreases with increase in temperature indicating the reduction of grain and grain boundaries resistance. The frequency at which Z^1 becomes independent of frequency has been shifted towards higher frequency side with raise in temperature, shows the presence of frequency relaxation process in the material. Further, the magnitude of Z' decreases with increase in both frequency as well as temperature indicates the increase in AC conductivity of the material. Further, the Z' values merges above10KHz at all temperatures.

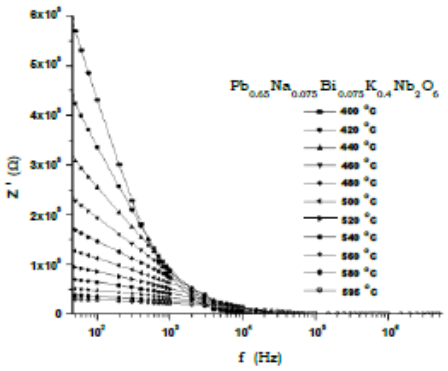

Fig5. *The variation of real part of the impedance (Z') as a function of frequency at different temperatures*

The variation of imaginary part of impedance (Z^{11}) with frequency at different temperatures has been shown in figure 6. The Z^{11} values reach a peak value with frequency for temperatures above 400^0C. For temperatures below 400^0C the peak was beyond the range of frequency of measurement under study. The asymmetric broadening of the peaks suggests the presence of electrical process in the spread of relaxation time.

The peak (Z^{11}_{max}) seems to shifts towards higher frequencies side with increasing temperature indicating increasing the relaxation, increase in loss in the material and dependence of space charges on temperature and frequency. The relaxation times, τ were calculated from the frequencies at which the Z^{11}_{max} is observed. Hence, the magnitude of Z^1 as well as Z^{11} decreases with increase in frequency.

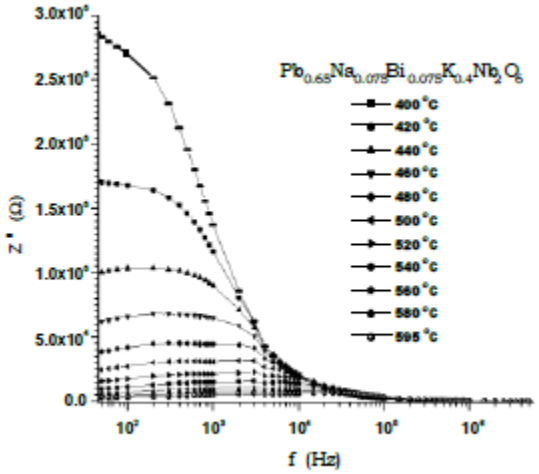

Fig6. *The variation of imaginary part of impedance (Z^{ll}) with frequency at different temperatures.*

From the figure 6 irrespective of the temperature at which measurements were made, all the curves merge above 10 KHz. Since, the space charge polarization is reduced with increasing frequency [24]. At higher frequencies, the contribution from the grain predominates owing to the absence of the space charge effects.

The peak heights are proportional to grain [or] bulk resistance, R_b according to the equation,

$Z^{11} = R_b\ [\omega\tau / (1+ (\omega\tau)^2]$ in the Z^{11} versus frequency plots [25].

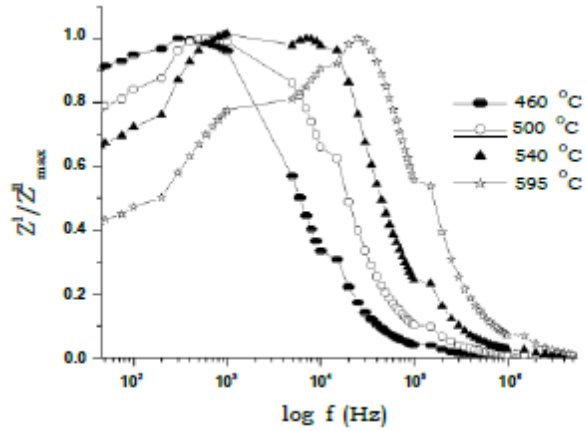

Fig7. *The normalized imaginary part Z^{ll} / Z^{ll}_{max} of impedance as a function of frequency at several temperatures.*

Figure7 shows the normalized imaginary part Z^{ll} / Z^{ll}_{max} of impedance as a function of frequency at several temperatures. It seems from the figure that at higher temperature trigger

another relaxation process. The normalization parameter, $Z^{II} / Z^{II}{}_{max}$ exhibits a peak in slightly asymmetric degree at each temperature especially at high temperatures. At the peak the relaxation is defined by the condition

$\omega_m\tau_m = 1$

Where, τ_m is relaxation time at the peak. Figure 8 shows the relaxation frequency obeys the Arrhenius relation given by

$\omega_m = \omega_0 \exp [-E_\tau / K_B T]$

Where, ω_0 is pre-exponential factor. The activation energy E_τ calculated from the $\log\omega_m - 1/T$ data. The activation energies are given in table3.

Table3. *Activation energies calculated from log ω_m -1/T data*

Composition	Temperature Range (^{0}C)	Activation energies (eV)
PNBKN	595-500	0.75
	480-400	0.37

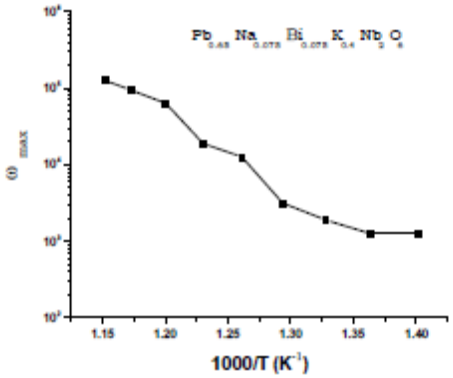

Fig8. *Temperature dependence of relaxational frequency*

Electrical properties of electroceramics at fixed frequency don't give a whole set of properties towards the evaluation of the electric parameters as a function of temperature. Electroceramic materials show a variety of frequency dependent phenomena associated with grain boundaries region and intrinsic properties of material [26-28]. Knowing the frequency dependence of Z^I and Z^{II}, one can determine the spread of the relaxation times by using circular diagrams suggested by Cole-Cole.

It is the representation form of the dielectric dispersion in graphical form, which relates real part of impedance Z^I at various frequencies. Given the same relaxation time Z^I and Z^{II} points that obey fall on the semicircle with its center lying on the axis of real part of impedance. If the dipoles differ in relaxation time they take shape of semicircular arc with its center below the real axis with center equal to $\varphi\pi/2$, where φ is the depression angle with the real axis.

The impedance data can be represented as an equivalent circuit consisting of two parallel RC elements in series [29, 30]. This is the one of the most common interpretation for polycrystalline materials having a contribution of grain (bulk) and grain boundary in series. The impedance of the circuit is given by [31]

$Z^* = [1/R_g + j\omega C_g]^{-1} + [1/R_{gb} + j\omega C_{gb}]^{-1}$

Where, R and C represents resistance and capacitance, the subscript g and gb refers to grain and grain boundary respectively. The frequency at the semicircle maxima, ω_{max}, and, correspondingly, at the Debye peak maxima, for each RC element is given by

$\omega_{max} = 2\pi f_{max} = (RC)^{-1} = \tau^{-1}$

Where, the product RC is the time constant, τ, of the RC element; τ and therefore, f_{max} are

intrinsic properties of the RC element, because they are independent of geometry [32] of the material.

Generally, the arc at high frequency end refers to bulk and at low frequency end refers to grain boundary. The resistance of bulk or grain (Rg), grain boundary (Rgb) could directly be obtained from intercept on the Zl axis. The capacitance of grain and grain boundary (C_g, C_{gb}) due to these effects can be calculated using the relation,ωRC=1,where, ω is the angular frequency at the maxima of the semicircle for the component. Cole-Cole plots of impedance at different temperatures (420-595^{0}C) has been shown in figure.9 (a). A straight-line response has been observed below 400^{0}C. As the temperature increases the slope of the line decreases and which makes a curve towards the x- axis. Temperature above 420^{0}C, the curve becomes almost semicircle which can be resolved into two indicating the increase in conductivity of the material. Also, the centers of semi circles that compose the total electric response are centered below the real axis, making an angle φ with x- axis (non –Debye type). Figure 9 (b) shows the Nyquist plot of PNBKN at 560^{0}C.

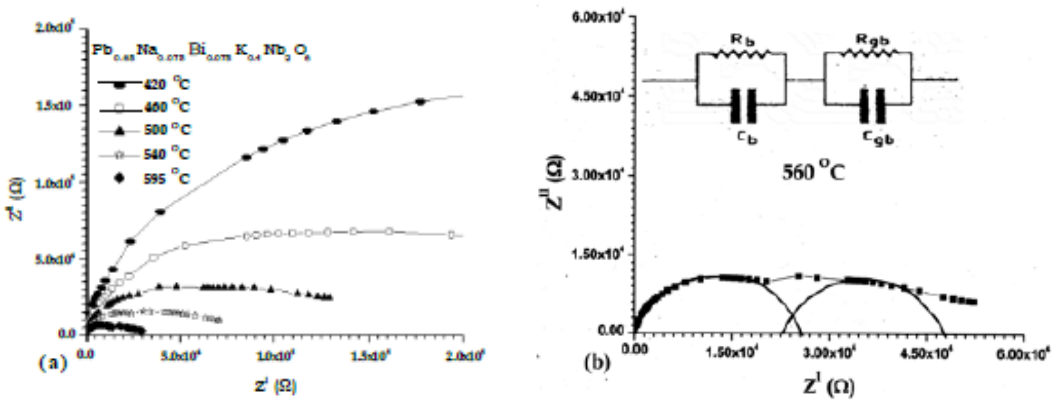

Fig9. *(a)Cole-Cole plots (b) Nyquist plot of PNBKN at 560^{0}C*

The appearance of two semi circles in the Cole-Cole plots indicates that there are two relaxational mechanisms, which may be due to grain and grain boundary. Also, poor separation of this overlapped semi circles is ascribed to the pore size. It is known that [33], in electroceramics, if the pore size is greater than 1μm, it would lead to the overlapping of the semi circles. As the temperature increases all the semicircles became smaller and shift towards lower Z^1 values indicating a reduction in the resistance of both the grain and grain boundary.

At higher temperatures (≥420^{0}C) two semicircles could be obtained with different values of resistance for grain and grain boundary. Hence, grain and grain boundary effects could be separated at these temperatures. A sharp decrease in dielectric constant with the increase in frequency can be explained in terms of interfacial polarization. In case of polycrystalline ceramics, this is commonly grain boundaries are insulating. The semi conductive grains in ceramic is believed to loose traces of oxygen during sintering at high temperature as per the reaction [34],

$$O_0 \rightarrow \tfrac{1}{2}\, O_2\uparrow + V_0'' + 2e^-$$

Where, all the species are written according to Kroger Vink notation of defects. These defects affect impedance and capacitance in the formation of barrier layers at the grain –grain boundary interface [34]. During cooling of the samples after sintering re- oxidation takes place. This oxidation is limited to surface and grain boundaries only due to insufficient time. These results in difference between resistance of grain boundary and grain, giving rise to barrier [35].The build – up of charge carriers at grain – grain boundary interface causes large polarization resulting in high dielectric constant at lower frequencies. Fig. 10 shows variation of grain, grain boundary (a) Resistance (b) Capacitance (c) Relaxation with temperature. Grain and grain boundary conduction and relaxation activation energies are tabulated in table 4.

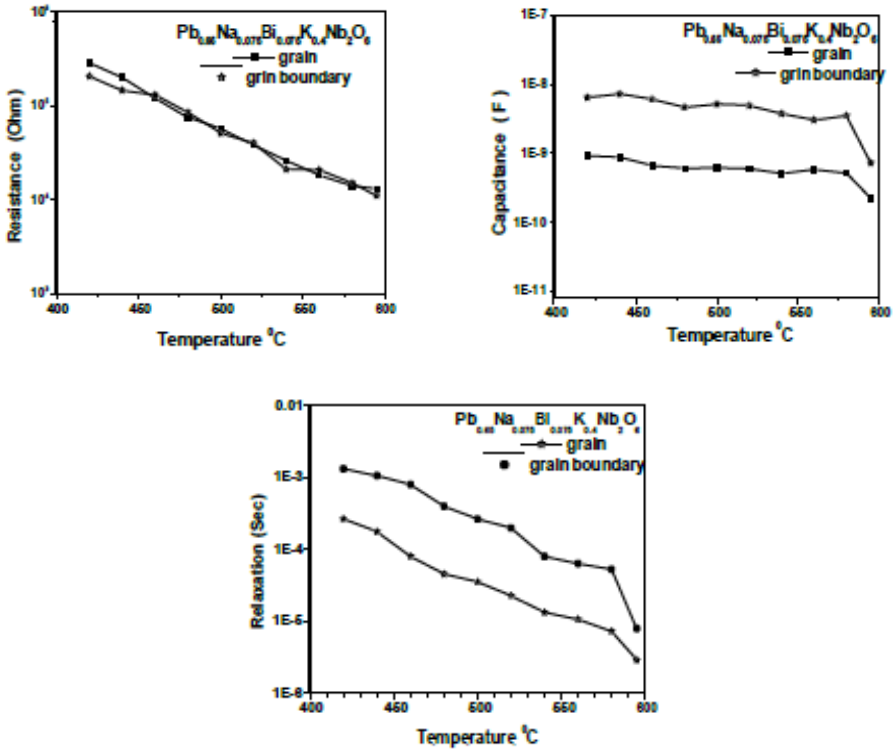

Fig10. *Variation of grain, grain boundary (a) (top) Resistance (b) (middle) Capacitance (c) (Bottom) Relaxation with temperature*

Table4. *Activation energy values (eV) of conduction (E) and relaxation (e) for grain(g) and grain boundary (gb).*

Composition	Temperature	Grain conduction activation energy, E_g(eV)	Grain boundary conduction activation energy, E_{gb}, (eV)	Grain relaxation activation energy, eg(eV)	Grain boundary relaxation activation energy, e_{gb} (eV)
PNBKN	500-560^{0}C	0.44	0.49	0.29	0.26

5. MODULUS SPECTROSCOPY

From the physical point of view, the electrical modulus corresponds to the relaxation of the electrical field in the material when the electric displacement remains constant. Therefore, the modulus represents the real dielectric relaxation process [36]**.** The usefulness of the modulus representation in the analysis of relaxation properties was demonstrated both for ionic conductors [37] and polycrystalline ceramics [38]. In practice, regions of low capacitance , such as grain interiors, are characterized using M'' data, where as more resistive regions, such as grain boundaries and pellet surface layers, which often have higher associated capacitances, are characterized using Z spectra [39]**.**

The complex electrical modulus is a parameter that can be expressed as Fourier transform function $\Phi(t)$ gives the time evolution of electric field with in the dielectric, $\boldsymbol{\varepsilon^* = \varepsilon - i\,\varepsilon}$

$$\mathbf{M^*(\omega) = 1/\varepsilon^* = M'(\omega) + i\,M''(\omega)}$$

$$= \mathbf{M_\infty\,[1 - \int exp\,(-i\omega t)\,(d\Phi(t)/dt)]}$$

$$= \mathbf{(\varepsilon' + i\,\varepsilon'')/\varepsilon'^2 + \varepsilon''^2}$$

Variations of real (M^l) part of electrical modulus with frequency (45Hz-5MHz) at various temperatures (30^0-595^0C) have been shown in Figure 11. At a constant temperature, M^l increases with increase in frequency and takes nearly a constant value. At low frequency and high temperature region, M^l approaches zero confirming an appreciable electrode and /or ionic

polarization [40].

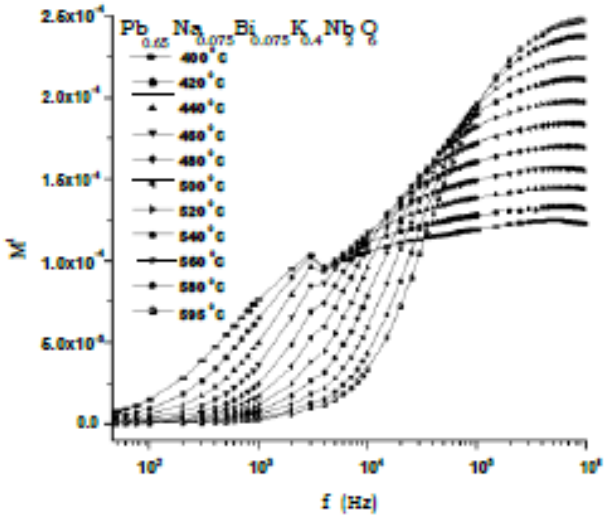

Fig11. *Variation of real part of electrical modulus with frequency*

Figure 12 shows the variation of imaginary part of modulus (M^{II}) with frequency at various temperatures (400^0 – 590^0C). As the temperature increases peak frequency of M^{II} shifts to higher frequency side. The low frequency side of peak represents the range of frequency in which the ions can move over long distances, i.e ions can perform successful hopping from one site to the neighboring site. The high frequency side of M'' peak represents the range of frequency in which the ions are strictly confined to their potential wells and ions can make only localized motion with in the wells [41-44].

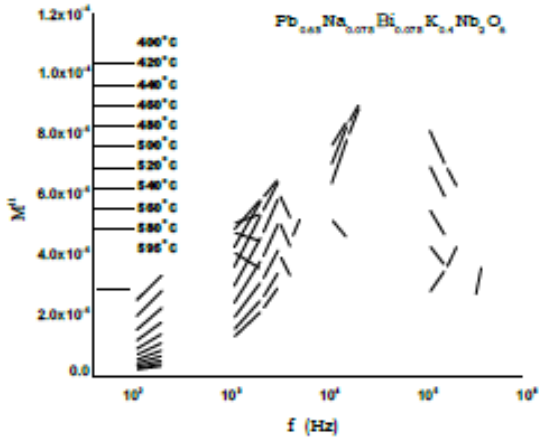

Fig12. *The variation of imaginary part of modulus (M^{II}) with frequency at various temperatures*

The shift in frequency of $M^{''}$ peak corresponds to the so called conductivity relaxation. Since the change in the dielectric constant of the grain boundary phase is relatively small (almost constant) with temperature, the change in the value of M'' indicates the grain contribution. The activation energies of D.C conduction can be obtained from Arrhenius plot of M'' peak frequencies. The reciprocal of frequency of M'' peak represent the time scale of transition from long range of mobility and is defined as the characteristic relaxation time, τ_p. Figure 13 shows the Arrhenius plot, relaxation angular frequency, $\omega_p = \omega_0 \exp [-E_\mu / K T]$ as a function of inverse of temperature, where ω_0, τ_0 and T are the pre exponential factors of angular frequency, relaxation time and absolute temperature.

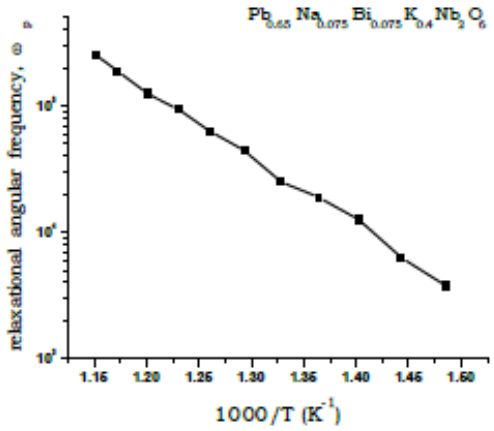

Fig13. *The Arrhenius plot of relaxation frequency as a function of 1/T*

The activation energies obtained from Arrhenius plots of relaxation angular frequency. The values of activation energies are tabulated in table 5.

Table5. *Activation energies of relaxation energies frequencies from M″ peaks as a function of 1/T*

composition	Temperature range (^{0}C)	DC conduction activation energies (eV)
PNBKN	595-500 480-400	0.55 0.48

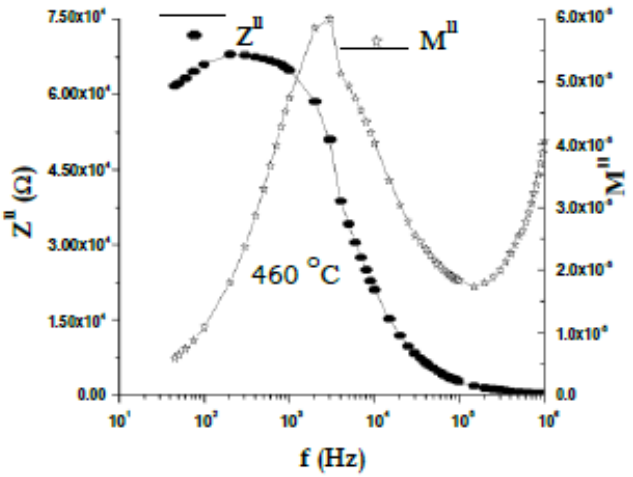

Fig14. *Representation of Z" and M" as a function of frequency at 460^{0}C.*

The representations of Z" and M" as a function of frequency at 46^{0}C have shown in the figure 14. These representations of Z" and M" permit analysis of apparent polarization (space charge) by inspection of the magnitude of mismatch between the peaks of the both parameters. A significant mismatch was observed in Z" and M" peaks in the measured frequency range. This significant mismatch of Z" and M" peaks indicates the presence of Maxwell-Wagner type space charge polarization arising at defects (grain boundaries, sample-electrode interfaces) present in the sample. The frequency explicit plots of Z" and M" indicates departures from the ideal Debye behavior. In ideal case the Z" and M" peaks should be coincident on the frequency scale [45].

6. DC AND AC CONDUCTIVITY

Figure 15 shows the thermal behaviour of ac conductivity σ(ω)of PNBKN with frequency at different temperatures. The variation of σ(ω) with frequency shows flattening with the increment in temperature i.e., above 420^{0}C in PNBKN. The switch from the frequency – independent σ_{dc} to frequency dependent σ(ω) regions show the one set of the conductivity relaxation phenomenon

and the translation from the long range hopping to the short range ion motion [46].

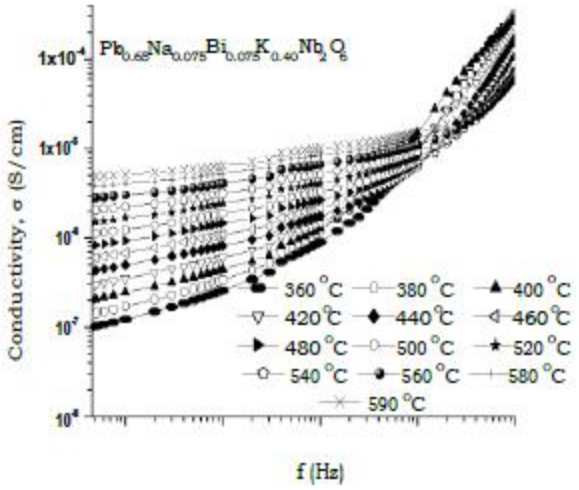

Fig15. *Variation AC conductivity as function frequency at different temperatures*

Figure 16 shows the thermal behaviour of dc and ac conductivity of PNBKN at different frequencies. The conductivity activation energy values are evaluated at different temperature regions and frequencies. Non linearity of the curve (figure 16) indicates the conduction process in the compound is of mixed type. The conducting species may be electrons in the low temperature and defects in high temperature range. These vacant sites act as the trapping centre for the mobile charge carriers and conduct parallel to the oxygen ions and hence the conductivity of the sample increases in the high temperature region by hopping mechanism of the charge carriers among the available vacant sites. A small flat region observed in the temperature range 300-225^{0}C become more flat at further low temperatures reflects the conductivity is independent of temperature. Similar behaviour has been reported [47] in TB structure $Na_2Pb_2Eu_2W_2Ti_4O_{30}$ ceramics.

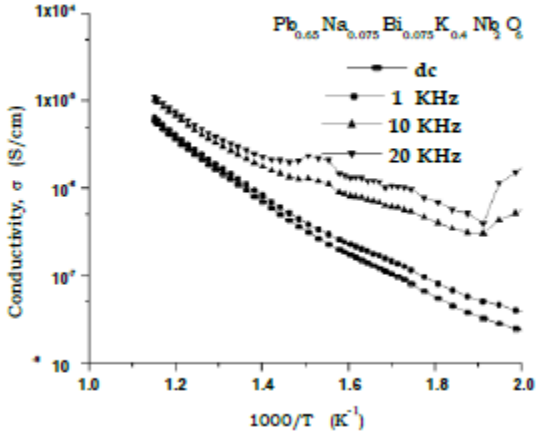

Fig16. *Variation of DC and AC conductivity as*

Also, an anomaly has been observed at a particular dielectric response of the material with temperature shows spontaneous polarization due to permanent dipoles present in the system. Their presence can also be seen from the dc conductivity response and from the changes in slope. The dc conductivity increases with increase in temperature and shows nearly constant conduction at low temperatures. This shows that the compound has negative temperature coefficient of resistance characteristic. At high temperature (>575^{0}C) all the conductivity curves obtained at different frequencies are found to merge. This type of behaviour is also found in PKN [12] compositions. It may be attributed to the long range electrostatic force, resulting from the spontaneous polarization of the sample, mobility and tendency to cancel the short range forces,

which arises from attraction and repulsion between the neighboring ions. Table 6 shows the dc and ac conductivity activation energy values of PNBKN.

Table6. *D.C and A.C conductivity activation energy values of PNBKN*

Temperature range (^{0}C)	Conductivity Activation Energy (eV)			
	dc	ac		
		1kHz	10kHz	20kHz
590-460	0.37	0.37	0.24	0.24
440-370	0.23	0.26	0.15	0.06
310-260	0.21	0.17	0.13	0.018

The resistivity in ferroelectrics compounds is known to be due to formation of small polarons. The electrons associate with small polarons spends most of its time trapped on a single ion. For the conduction due to small polarons the following relation is expected to hold good [48]

$$\sigma_{ac} = \sigma_{dc} + \omega^2\tau^2 / (1+\omega^2\tau^2)$$

Where, τ is the staying time of a polaron. For ω up to 1MHz, the $\omega^2\tau^2 <1$ and the above equation expressed as

$$\sigma_{ac} - \sigma_{dc} = \omega^2\tau^2$$

The conductivity is found to increase with increase in frequency. Variation of log (σ_{ac}-σ_{dc}) as a function of log ω^2 has been shown in figure4.6.3. The linear variation of the plot confirms the polaron hoping mechanism.

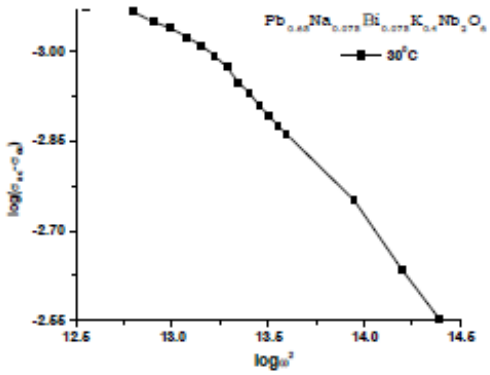

Fig17. *Variation of log(σ_{ac}-σ_{dc}) as a function of log ω^2*

7. CONCLUSIONS

Polycrystalline lead compound $Pb_{0.65}Na_{0.075}Bi_{0.075}Nb_2O_6$ generally formulated as $Pb_{1-x-y}(Na_{0.5}Bi_{0.5})_yK_{2x}Nb_2O_6$ where x = 0.20 and y = 0.15 has been synthesized and fabricated. At room temperature the compound ($Pb_{1-x-y}(Na_{0.5}Bi_{0.5})_yK_{2x}Nb_2O_6$ where x = 0.20 and y = 0.15) exhibited orthorhombic structure. Dielectric analysis reveals the presence of electrode polarization, free charge motion at low frequencies which are related to space charge polarization and conductivity relaxation. Temperature dependent critical exponent n(T) shows a minimum at T_C. Cole-Cole plots of impedance in PNBKN ceramic reveals the relaxation is non Debye type. The shift in the peak frequency of M" indicates the presence of temperature relaxation process in the material. The linear variation in the plot of log(σ_{ac}-σ_{dc}) as a function of log ω^2 at 30 ^OC confirms the polaron hoping mechanism.

REFERENCES

[1] T.Yamada, Appl. Phys. Lett. **23** (1973) 213, J. Appl. Phys., **46** (1975) 2864.

[2] Yamauchi. H, Appl. Phys. Lett.., **32** (1978)599.

[3] Neurgaonkar.R.R, Hall.W.F, Cory.W.K, Oliver.J.RSharp.E.J, WoodG.L, Miller. M.J,ClarkIII.W.W, and Salamo.G.J,Mar. Res.Bull, **23** (1988) 1459.

[4] Elaatmani.M, Zegzouti.A, Ravez.J and Hagenmuller.P, Rev. Chi. Min, **23** (1986)290.

[5] Ravez. J and Elouadi.B, Mat. Res. Bull., **10** (1975) 1249.

[6] Giess. E.A, Scott. B. A, Burns. G, O'kone. D. F, and Semuller. A. J, J. Ame. Cer. Soc., **52** (1969) 276.

[7] Bhanumathi. A, Narayana Murthy. S, Umakantham. K, Chandra Mouli. K, Padmavathi. G, Tirumala Rao. K, Syamalamba. V, Ferroelectrics, **102** (1990) 173.

[8] W.E.Kramer and G.W.Roland, J. Crystal Growth, **58** (1982) 393.

[9] P.Jana, V.A.Kallur, M.A.Drummond, S.Nigli and R.K.Pandey, Proceedings of the Eighth IEEE International Symposium on the Applications of Ferroelectrics, IASF '92, Greenville, SC, 374 (1993).

[10] A.Smith, J.F.Baumard, P.Abelard and M. F. Denanot, J. Appl. Phys. **65** (1989) 5119.

[11] S.P.Jiang, J.G.Love and S. P. S. Badwal, in Electrical properties of Oxide materials, Key Engineering materials, Vol 125-126, Edited by J.Nowotny and C.C.Sorrell (Trans. Tec. Pub.,Switzerland, 1997), p.81.

[12] K. Sambasiva Rao, P. Murali Krishna, T. Sci. & Eng. B, **131** (2006) 127.

[13] A. R.West, "Solid State Chemistry and its Applications", John Wiely and Sons, 1987.

[14] U. Fluckiger, H. Arend and H. R. Oswald, Ceram. Bul. **56,** (1977) 575.

[15] P.Jana and R. K. Pandey, Proceedings of the Eighth International meeting on Ferroelectricity, 1993.

[16] K. Sambasiva Rao, T. N. V. K. V. Prasad, N.Vallinath, J.H.Lee and Sang Hee Cho, Ferroelectric letters, **30** (2003) 25.

[17] T. R. Shrout, H. Chenand L. E. Cross, Ferroelectric letters,**74 (**1987) 317.

[18] W. K. Lee, J. F. Liu, A. S. Nowick, Phys. Rev. Lett. **67** (1991) 1559.

[19] Z. Lu, J. P. Bonnet, J. Ravez, P. Hagenmuller, Solid State Ionics **57** (1992) 235.

[20] S. Lanfredi, P. S. Saia, R. Lebullerger, A. C. Hernands, Solid. State Ionics, **146**, (2002) 329.

[21] R. Gerhardt, J. Phys. Chem. Solids, **55** (1994) 1491.

[22] Ashok Kumar, B. P. Singh, R. N. P. Choudhary, Awalendra K. Thakur, J. Alloys and compounds **394**, (2005) 292.

[23] B. V. Bahuguna Saradhi, K. Srinivas, G. Prasad, S. V. Suryanarayana and T. Bhimasankaram, Materials Science and Engineering B **98**, (2003) 10.

[24] C. L. Fan, D. Ciardullo and W. Huebrier, Mater Sci &Eng B **1009**, (2003) 1.

[25] R. Von Hipple, Dielectric and Waves (NY): John – Wiley Sons (1954).

[26] M. A. L .Nobre,. S. Lan fredi, Mater. Lett. **50**, (2001) 322.

[27] M. A. L. Nobre, S. Lan fredi, J. Phys. Chem.Solids. **62**, (2001) 1999.

[28] M. A. L. Nobre, S .Lan fredi, Mater.Lett. **47**, (2001) 362.

[29] J R. Macdonald, in Impedance Spectroscopy (NY: Wiley), (1987).

[30] I. M. Hodge, M. D. Ingram and A. R. West, J. Amer. Cera. Soc., **74** (1976) 125.

[31] R. P. Tandon, J. Korean Phy. Soc, **32**, (1998)327.

[32] A. R. West, D. C. Sinclair and N. Hirose, J.Electroceram., **1 (1)** (1975) 65.

[33] M. C. Steil, F. Thevenot and M. Kleitz J. Electrochem. Soc., **144** (1997) 390.

[34] F. A. Kroger and H. J. Vink, Solid State Physics, **3,** (1956) 307.

[35] DaRen Chen and Y. G. Yan, Electronic Elements Materials **1** (1982) 25.

[36] H.Wagner and R.Richert , Polymer, **38,** (1997) 5801.

[37] P. B. Macdo, C. T. Moynihan and R. Bose, Phys.Chem.Glsses**13** (1972) 171.

[38] J. Liu, Ch-G Duan, W. G.Yin,W, NMei R. W. Smith and J. R. Harday J. Chem. Phys. **119** (2003) 2812.

[39] N. Hirose, and A. R. West, J. Am. Ceram. Soc.**79** (1996) 1633.

[40] Jin Soo Kim and Tae Kwon Song, J. Phy. Soc. Japan **70** (2001) 3419.

[41] R. L. Nagai and C.Leon: Solid State Ionics **125** (1999) 81.

[42] P. Pissis and A.Kyritsis: Solid State Ionics **97** (1997)105.

[43] V. V. Shilov, V.V.Shevchenko, P. Pissis, A. Kyritsis, G. Georgoussis, Yu. P. Gommza, S. DNesin and N.S.Klimeko:J.Non- Cryst.Solids, **275** (2000) 116.

[44] D. L. Sidebottom, P. F. Green and R. K. Brow: J. Non-Cryst. Solids, **183**(1995) 151.

[45] A. R. James, S. Priya, K. Uchino and K. Srinivas, **90** (2001) 3504.

[46] R. Mizaras, M.Talashige, N.Banys, S. Kojima, J. Grigas, Hamazaki, Sin-Ichi and A. Brilingas, J. Phys. Soc. Japan, **66** (1997) 2881.

[47] P. R. Das, R. N. P Chowdary, B. K. Samantray, Porce. NSAE, (2006) 176.

[48] D. Alder, J. Feinleib, Phy.Rev.B, **2** (1970) 3112.